Available online at www.sciencedirect.com
ScienceDirect
C. R. Physique 8 (2007) 806–820
COMPTES RENDUS PHYSIQUE
http://france.elsevier.com/direct/COMREN/

Neutron scattering/Diffusion de neutrons

Mapping residual and internal stress in materials by neutron diffraction

Philip J. Withers

Manchester Materials Science, University of Manchester, Grosvenor St., Manchester, M1 7HS, UK

Available online 19 November 2007

Abstract

Neutron diffraction provides one of the few means of mapping residual stresses deep within the bulk of materials and components. This article reviews the basic scientific methodology by which internal strains and stresses are inferred from recorded diffraction peaks. Both conventional angular scans and time-of-flight measurements are reviewed and compared. Their complementarity with analogous synchrotron X-ray methods is also highlighted. For measurements to be exploited in structural integrity calculations underpinning the safe operation of engineering components, measurement standards have been defined and the major findings are summarised. Examples are used to highlight the unique capabilities of the method showing how it can provide insights ranging from the basic physics of slip mechanisms in hexagonal polycrystalline materials, through the materials optimisation of stress induced transformations in smart nanomaterials, to the industrial introduction of novel friction welding processes exploiting stress residual measurements transferred from prototype sub-scale tests to the joining of full-scale aeroengine assemblies. ***To cite this article: P.J. Withers, C. R. Physique 8 (2007).***
© 2007 Académie des sciences. Published by Elsevier Masson SAS. All rights reserved.

Résumé

Cartographie des contraintes résiduelles et internes dans les matériaux par diffraction de neutrons. La diffraction de neutrons est une des rares techniques permettant de cartographier en profondeur les contraintes résiduelles dans les matériaux. Cet article présente une revue des bases de la méthodologie scientifique qui permet de déduire les déformations et contraintes internes des mesures de pics de diffraction. Les méthodes conventionnelles par balayage en fonction de l'angle et les mesures par temps de vol sont décrites et comparées. On insiste sur leur complémentarité avec les méthodes analogues utilisant le rayonnement synchrotron. Pour que ces mesures puissent être utilisées dans les calculs d'intégrité structurale nécessaires à une utilisation sûre des composants mécaniques, une méthodologie standard a été définie et est résumée ici. Des exemples mettent en valeur le potentiel unique de la méthode, montrant comment elle permet d'obtenir des informations allant des mécanismes de base du glissement dans les matériaux hexagonaux polycristallins, à l'optimisation de matériaux par des transformations structurales induites par les contraintes, et à la validation industrielle des nouveaux procédés de soudage par friction appliqués aux assemblages de composants aéronautiques. ***Pour citer cet article : P.J. Withers, C. R. Physique 8 (2007).***
© 2007 Académie des sciences. Published by Elsevier Masson SAS. All rights reserved.

Keywords: Residual stress; Structural integrity; Neutron diffraction; Smart materials; Composites; Welding

Mots-clés : Contraintes résiduelles ; Intégrité structurale ; Diffraction de neutrons ; Soudage

E-mail address: philip.withers@manchester.ac.uk.

1631-0705/$ – see front matter © 2007 Académie des sciences. Published by Elsevier Masson SAS. All rights reserved.
doi:10.1016/j.crhy.2007.09.015

1. Introduction

Almost as soon as X-ray Bragg diffraction had been developed as a tool for measuring the lattice spacings of crystals [1], its potential as a means of measuring elastic strain was identified in a series of articles [2–4], as retold in a comprehensive review of its historical development by Hauk [5]. The opportunity to probe the state of elastic strain and hence stress in the bulk of materials had to wait until suitable thermal neutron beams became available at research reactors. The first papers appeared in 1981 by Allen et al. [6], Pintschovius et al. [7] and Krawitz et al. [8]. More recently pulsed neutron sources have increased the level of information available, so that many lattice planes can be sampled simultaneously [9]. Neutron diffraction has now become an established tool for the measurement of residual stress deep inside a wide range of engineering components [9–11]. Today, high energy X-ray beams with penetrations not far short of those typical of thermal neutrons are available with the arrival of 3rd generation synchrotron X-ray sources providing a complementary tool [12,13]. This article reviews the basic scientific principles by which internal strain in a given direction can be deduced from peaks recorded by neutron diffraction. By making a number of strain measurements in different directions, but at the same location, it is possible to derive the tensors describing the elastic strain and hence stress at that location. In this review, the contribution of neutron diffraction strain measurement for basic physics, materials science and engineering is illustrated with reference to examples ranging from examinations of the basic mechanisms of slip at the atomic level to the introduction of new industrial joining process at the full industrial component scale.

At this point it is probably worth defining what are meant by internal and residual strains and stresses. The terms internal stress and strain will be used by the author to describe stresses/elastic strains that are additional to those needed to satisfy equilibrium. In other words they are self-equilibrating, such as might arise between the phases of an aligned fibre composite under uni-axial tensile load. For stiff fibres, the fibres would be stressed more than the average stress, while the matrix would be stressed less. As a result, internal stress components always average to zero over the whole body, or over any particular cut through the body. In the present example, the fibres have tensile axial internal stresses; the matrix compressive ones on average. In this case, provided the composite was not strained beyond its elastic limit, these internal stresses would fall to zero as the composite was unloaded. Residual stresses are a special case, being self-equilibrating stresses that exist within a stationary solid body when no external forces are acting. Since internal stresses self-equilibrate they are not usually immediately apparent, can be difficult to measure, are hard to predict, and can give rise to unexpected failure if not accounted for.

2. Basic scientific methodology

Diffraction can provide a unique insight into elastic strains. The approach rests on the fundamental relation [1] between the wavelength of the radiation, λ, the distance between selected lattice planes *hkl* in a crystalline material, d_{hkl}, and the angle, $2\theta_{hkl}$, at which the radiation is scattered coherently and elastically:

$$2d_{hkl}\sin\theta_{hkl} = \lambda \tag{1}$$

This allows one to measure lattice spacings and hence the elastic strain in a direction normal to the lattice planes via deviations from the unstressed spacing. In a sense the crystal lattice, which constitutes a natural building block of crystalline solids, is adopted as a natural and ever-present *atomic plane strain gauge* embedded in each crystallite, or grain.

Internal stresses can be divided into three categories by scale; type I macrostresses varying at the continuum scale, type II microstresses at the grain scale and type III microstresses at the atomic scale. As a result each can be assigned a characteristic length scale: L_0, corresponding to the length over which the stress averages to zero. In simple terms $L_0^{\mathrm{I}} \sim$ sample dimensions; $L_0^{\mathrm{II}} \sim$ few grain diameters and $L_0^{\mathrm{III}} \sim$ tens of atom spacings.

No measurement technique can measure the strain at a single point in a component sample. Diffraction techniques measure strain averaged over a sampled gauge volume, V_v, usually defined by apertures or collimators (Fig. 1). Typical sizes of the sampled gauge volume can range from 0.2 to 1000 mm^3. If the sampled gauge volume, V_v, is finer than the characteristic volume ($V_0 \sim L_0^3$ [14]) then variations in strain will be recorded as shifts in the diffraction peak positions. If on the other hand it is greater than the characteristic volume, then the corresponding strain will not be measured since it averages to zero over this region. Since the sampled gauge volume is usually much larger than the grain size, as indeed it must be for true powder diffraction, it is also much larger than the characteristic volumes

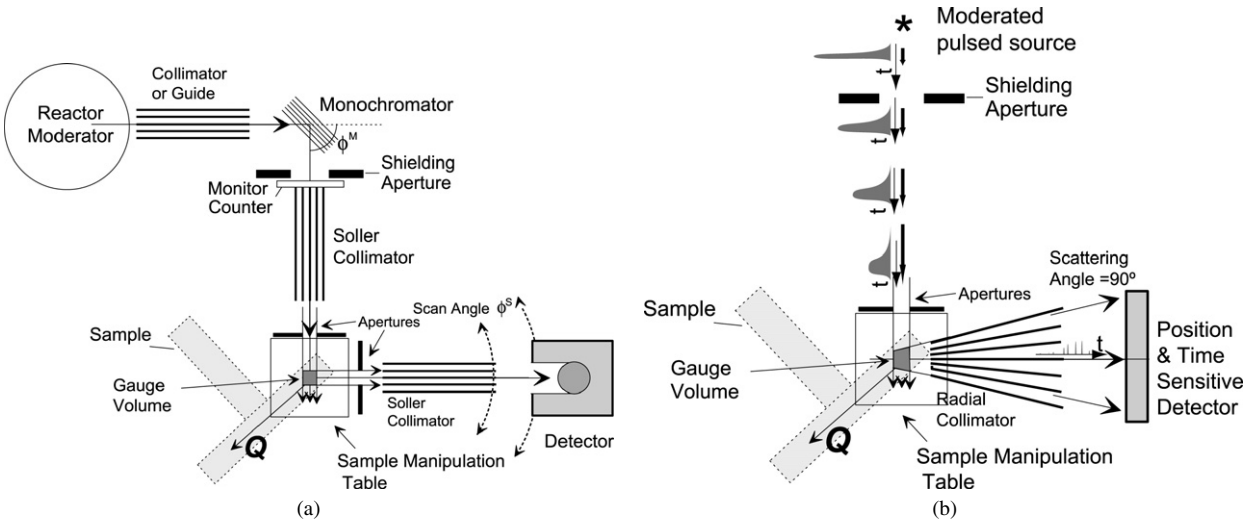

Fig. 1. (a) Conventional monochromatic two theta scanning as practised at a constant flux source; (b) time-of-flight instrument as might be found at a pulsed spallation source. In both cases the strain is measured in the direction of the **Q** vector.

for type II and III microstresses. Thus microstresses, for which V_0^{II} and $V_0^{\mathrm{III}} < V_v$, normally give rise only to peak broadening.

3. Conventional angular scans and time-of-flight measurements

There are two basic designs of strain instrument: conventional angular scanning and time-of-flight [9]. While there are exceptions the former are traditionally located on monochromatic reactor-based sources, while the latter are located on pulsed white beam spallation sources.

3.1. Monochromatic angular scanning

This technique for measuring the lattice parameter is directly analogous to the much older X-ray diffraction method. It relies on the fact that elastic strain depends on the change in lattice spacing Δd_{hkl} obtained by differentiating Eq. (1) at constant wavelength:

$$\varepsilon_{hkl} = \Delta d_{hkl}/d^0_{hkl} = -\cot\theta^0_{hkl}\Delta\theta_{hkl} \tag{2}$$

where $\Delta\theta$ is in radians and d^0_{hkl} is the strain-free lattice spacing. While the best measurement accuracy is achieved as backscattering geometry is approached (2θ tends to π), it is more conventional to use a scattering angle of $\pi/2$ since this gives a cuboidal gauge volume (see Fig. 1(a)). In principle the whole diffraction profile could be obtained by scanning theta, but then different peaks would correspond to different strain directions. As a result, it is usual for the lattice strain, ε_{hkl}, for a single peak hkl to be measured. Theta scanning instruments are available at many facilities worldwide including at the ILL (SALSA), Grenoble [15]; Berlin & Munich [16]; Řež, Czech Republic [17]; Chalk River, Canada [18]; Petten, Netherlands [19]; Saclay, France [20]; Budapest [21]; NIST [22], MURR [18] and HFIR, Oak Ridge [18] in the USA. This approach is well-suited to macrostress mapping in cases where one or more individual representative peaks can be identified.

3.2. Time-of-flight method

Here the time-of-flight (tof) of each detected neutron is used to infer their velocity (= path travelled (L)/tof); from this their wavelength can be calculated. As a result a diffraction profile is recorded as a function of tof at a fixed scattering angle (usually 90°). Bragg's equation can be recast in terms of the tof t_{hkl} at which a peak is recorded:

$$d_{hkl} = \lambda_{hkl}/[2\sin\theta_{hkl}] = h.t_{hkl}/[2m_n L\sin\theta_{hkl}] \tag{3}$$

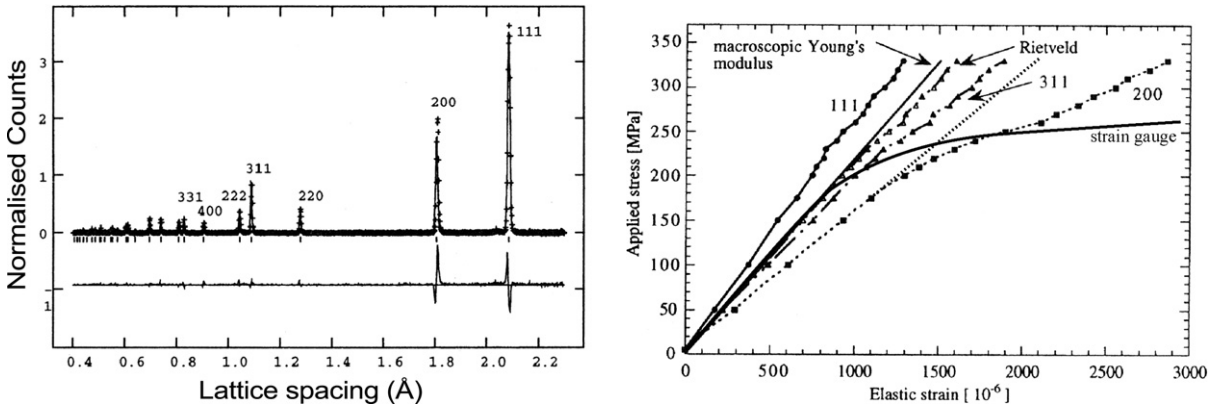

(a) (b)

Fig. 2. (a) A typical tof diffraction pattern for stainless steel under uniaxial loading of 340 MPa tensile stress. The fitted background has been subtracted, and the upper curve shows the experimental (crosses) and fitted Rietveld (line) profiles. Below is the difference curve on the same scale. It is seen that the fitted curve using an average lattice parameter does not account for the elastic anisotropy of the 111 and 200 peaks, which show a variance in opposite senses. (b) The corresponding elastic lattice strain response to the loading, as determined from individual peak analysis and by Rietveld analysis of the whole diffraction profile. The line given by the Rietveld analysis is approximately linear with stress throughout loading, being in good correspondence that of the macroscopic strain gauge in the elastic regime [24].

where m_n is the mass of the neutron and h is Planck's constant. This gives the strain in terms of the shift in the time at which the peak is recorded Δt_{hkl};

$$\varepsilon_{hkl} = \Delta d_{hkl}/d^0_{hkl} = \Delta t_{hkl}/t^0_{hkl} \tag{4}$$

For a white beam, diffraction from a given plane sweeps through in time from low scattering angles to high. This means that to define a gauge volume a radial collimator is required [23], as shown in Fig. 1(b). A typical tof profile is shown in Fig. 2(a). The peaks can be fitted individually, or collectively using a Rietveld [24] style refinement, to derive a single lattice parameter a_{hkl}. Examples of tof instruments include ENGIN-X at ISIS [25], POLDI on SINQ Switzerland [26], SMARTS at Los Alamos [18,27] and VULCAN at SNS [28]. This method is especially well suited to monitoring phase transformations or the mechanics of slip because of its capability to measure many peaks simultaneously.

3.3. Macro and intergranular stresses

That the lattice strain is proportional to the macroscopically applied stress, at least below the proportional (elastic) limit, is evident in Fig. 2(b). The figure also illustrates how the response of each lattice plane differs from the others, the strain gauge response and the Rietveld refinement, even at low loads. The different slopes of the stress–lattice strain curves before macroscopic plastic yielding is called *elastic anisotropy*, and arises from the anisotropic stiffness of a single crystal and the constraint each grain places on its neighbours as they try to deform according to the single crystal response. This means each lattice spacing varies in proportion to the applied stress, but has different diffraction elastic constants which are intermediate between the single crystal *hkl* values [29] and the isotropic bulk response.

The conversion from elastic strain to stress is analogous to Hooke's law

$$\sigma_{ij} = C_{ijkl}\varepsilon_{kl} = \frac{E_{hkl}}{1+\nu_{hkl}}\left(\varepsilon_{ij} + \frac{\nu_{hkl}}{1-2\nu_{hkl}}\varepsilon_{kk}\delta_{ij}\right) \tag{5}$$

where C_{ijkl} is the stiffness tensor and the quantities E_{hkl} and ν_{hkl} are the plane-specific analogues of Young's modulus and Poisson's ratio. These *hkl* specific diffraction elastic constants can be used to infer the macroscopic stress representative of the gauge volume, whereas the total stress in a grain (macroscopic stress plus the average type II intergranular stress) can be obtained by using the single crystal elastic constants.

It is also clear from Fig. 2(b) that, unlike a conventional strain gauge, to first order the lattice strains, which by their nature must be elastic, are not sensitive to macroscopic plastic strain. This is because plastic strain occurs by slip processes and the passage of dislocations through the crystalline lattice. This does not give rise to any increase in the

lattice spacing per se. However because each grain deforms plastically by different amounts according to its orientation this generates further intergranular misfit leading to type II intergranular stresses. These introduce non-linearities in the applied stress vs. lattice strain curves, as exemplified in Fig. 2(b) by the deviation of the 200 response from the dashed line. These non-linearities are termed *plastic anisotropy* and can lead to severe errors in the calculation of stress from strain if not accounted for [9,30]. The simplest course of action at a pulsed source is to use the Rietveld refinement which uses many diffraction peaks and tends to average out these deviations to give a value representative of the macroscopic response [24]. When using a monochromatic source it is advisable to choose reflections that are very nearly linear right through the elastic and plastic regimes, e.g. 311 in Fig. 2(b). The best peaks for a given material are recommended in the VAMAS standard procedure [31].

4. Complementary synchrotron methods

Third generation synchrotron sources provide access to high X-ray energies. At these high (hard) energies the attenuation length, defined as the path length over which the intensity falls to e^{-1}, increases markedly. This combined with the very high X-ray intensities they produce leads to path lengths of centimetres even in steel [32]. The main advantages are the high intensity and the high collimation of the beam, which allow data acquisition rates of the order of seconds if not milliseconds, and the definition of millimetre to micron size sampled gauge dimensions [33].

There are synchrotron X-ray instruments that are directly analogous to the theta scanning and tof neutron instruments described above. A typical theta scanning instrument is very similar to the design shown in Fig. 1(a), but it is common to use an analyser crystal on the diffracted beam prior to the detector rather than soller slits. These slits comprise a series of opaque parallel plates arranged edge-on to the beam to ensure that the transmitted beam is approximately parallel (Fig. 1(a)). With such rudimentary collimation the position of the diffraction peak is sensitive to movements in the centre of the scattering volume within the gauge volume. This occurs when the sample under investigation only partially fills the nominal gauge volume. This effect is well characterised and understood, and corrections have been developed to counter it [9]. It is not normally a great problem for neutrons because the method is primarily used to study stresses well within the body, but for synchrotron X-rays where the lower penetration and higher intensity make it well suited to near surface measurements, the use of an analyser crystal is recommended [34]. In essence, this acts like an extremely fine soller thereby improving the angular sensitivity and removing the sensitivity to position within the nominal gauge volume. Another difference is that diffraction peaks are often collected at very low diffraction angles, typically $2\theta = 5$ to 30°, rather than the approximately 90° angle conventionally used with neutrons. This is because at the short wavelengths (∼0.1 Å) associated with very high energy X-rays diffraction from low hkl planes occurs at such low angles.

Measurements by hard X-rays using theta scanning can provide very high spatial or time resolution measurements. A good example of the fast data acquisition timescales that can be achieved is provided by Stone et al. [35] who have followed the phase transformations that occur during the welding of steel by simulating the thermal excursion (20–900–20 °C) of weld filler metal having the composition given in Table 1, on the ID11 monochromatic beam instrument at the ESRF. By using a CCD area detector to collect complete diffraction rings downstream of the sample at low scattering angles (∼4–9°) acquisition rates of 0.1 s were employed per diffraction profile (Fig. 3(a)). By acquiring profiles throughout the heating and cooling experiment the hysteresis of the whole phase changes could be monitored over the whole thermal cycle (Fig. 3(b)).

Energy dispersive X-ray diffraction is directly analogous to the neutron tof method in that a large segment of the diffraction profile is collected simultaneously at a single scattering angle. Of course X-rays travel at the speed of light, but it is possible to measure the energy of a diffracted photon using a Ge detector. Consequently a Ge detector is placed downstream of the sample illuminated by a beam of hard X-rays (50–300 keV say) to detect diffracted photons usually at a scattering angle of around 5° [33]. Like the tof neutron method, it has the advantage that the whole profile is collected simultaneously [36]. As well as being well suited to studying phase transformations and intergranular stresses, it also means that very small gauge volumes can be interrogated in short times. In this way it can be used

Table 1
Composition (in wt%) of weld filler metal studied in Fig. 3

Fe	Ni	Mn	Mo	Cr	Si	C	N	O	V	Cu	Co	Ti	P	S	Nb	B
Bal.	2.95	1.90	0.61	0.43	0.21	0.048	0.030	0.027	0.021	0.02	0.017	0.010	0.009	0.006	0.003	0.0005

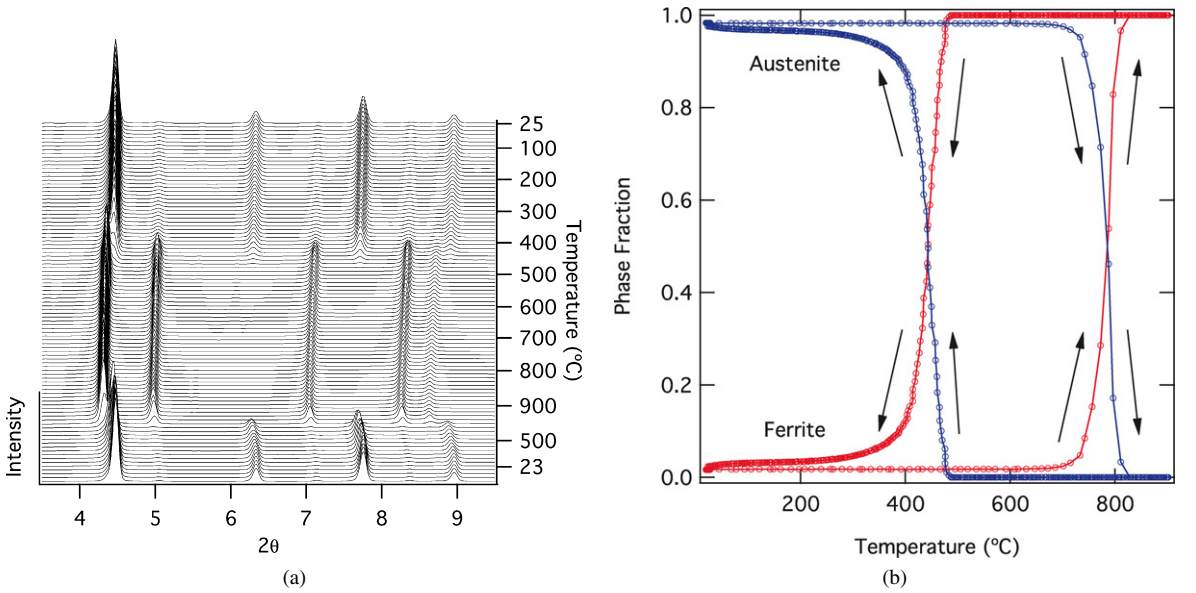

Fig. 3. (a) Weld filler metal having the composition given in Table 1 was heated to 900 °C (dwell 1 min) and then cooled at 1 C/s without constraint. Evolution of diffraction profile and (b) plot of phase hysteresis on ID11 at the ESRF using a monochromatic beam at 78 keV (wavelength 0.159 Å). For clarity, profiles in (a) are displaced vertically [35].

to build up a map of the residual stress piece-wise by translating the sample under the beam, for example around a crack tip. In a recent experiment a fatigue cracked 12 mm thick compact tension sample (Fig. 4(a) insert) made from extremely fine grained Al–Li alloy 5091 (Al–Li–Mg–C–O) was loaded to a nominally applied stress intensity of $K_{\max}^{\text{Appl}} = 6.6$ MPa $\sqrt{\text{m}}$ and the crack tip strain field observed on ID15 at the ESRF using a white beam. The scattering angle was 5° and the incident and diffracted apertures were 40 μm in size to give a 40 μm lateral spatial resolution [37]. The elastic strain and stress fields in the crack opening (loading) direction are shown in Fig. 4. By fitting the local elastic strain field to that predicted classically it was possible to infer the stress intensity actually experienced by the crack tip, rather than just that nominally applied, directly from the measurements.

In summary, the intense beams of high energy synchrotron X-rays available at synchrotron sources offer unparalleled spatial resolution lateral to the beam (1–100 μm) and fast data acquisition times (1 ms say). These make the method well suited to the collection of detailed maps of the strain field in two or three dimensions, or to monitor phase transformations where neutron diffraction would be unfeasibly slow. In counterpoint, there are serious drawbacks in the application of the synchrotron method. Firstly, the low scattering angles mean that the sampling gauge is usually very elongated. This means that the spatial variation is very different in different directions, being excellent lateral to the beam, but much poorer along the beam. Secondly, the low scattering angles mean that the method is well-suited to plate geometries where the significant stresses are in-plane, but for large or geometrically complex samples it can be difficult to achieve short path lengths for all measurement directions. Consequently it is often not possible to derive the stresses (which require at least 3 perpendicular strain values) without invoking simplifying assumptions, e.g. plane stress. As a solution researchers have developed hybrid methods whereby synchrotron diffraction is used to provide 2 components of strain and another method, e.g. neutron diffraction [38] used to determine the third. It should also be noted that neutron diffraction is often more appropriate for multiphase or composite materials containing both high and low atomic number elements. Finally, in many cases the high spatial resolutions achievable in theory cannot be realised in practice because the powder method breaks down due to insufficient grain sampling. Even at similar gauge dimensions to the neutron method, the very low divergence of the incident X-ray beam means that in many cases too few grains satisfy the diffraction condition to provide results representative of the bulk.

5. Measurements to rely upon

The prevention, prediction, or postponement of failure in components and structures upon the basis of sound physics is not just an interesting topic for research, it is essential for the safe execution of our daily lives. While the

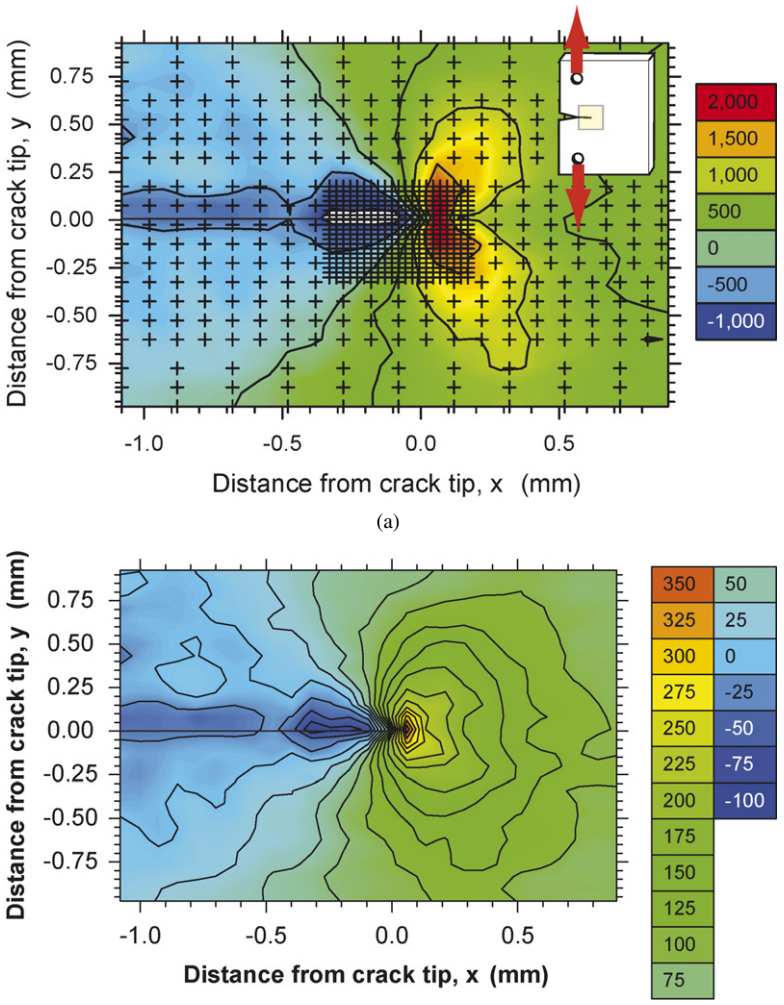

Fig. 4. (a) Crack opening (longitudinal) elastic strain, ε_{yy} (10^{-6}); and (b) stress, σ_{yy} (MPa) in a compact tension sample (see inset) loaded to a nominal stress intensity, $K_{\max}^{\text{Appl}} = 6.6$ MPa $\sqrt{\text{m}}$. Note the markers indicate the measurement positions for the coarse and finer maps; the crack tip is located at (0, 0) [37].

external loadings acting on a material or component are clearly important, other contributory factors include sub-optimal materials microstructure, pre-existing defects and residual stresses. In cases where failure cannot be tolerated, or where new processes, materials or fabrication procedures, leaner design or longer life prediction mean that a detailed knowledge of the residual stress is a commercial or social imperative. In such cases, the engineers must be able to justify the measurements they take against recognised standards.

In 2001, after a series of round robin studies an International Organisation for Standardisation Technology Trends Assessment document was produced recommending procedures for the measurement of residual stress by neutron diffraction in polycrystalline materials [31]. It outlines the method to be followed, calibration procedures, recommends diffraction peaks to be used for different materials, how to deal with elastic and plastic anisotropy (see earlier), methods for inferring the strain free lattice parameter and reporting guidelines.

A world wide round robin was undertaken in order to identify best practise [39]. Eighteen facilities worldwide participated in the study. It involved the measurement of the strain and stress distribution in a shrink-fit aluminium ring and plug sample. The sample comprised a ring of outer and inner diameters of 50 and 25 mm respectively, into which a plug, nominally oversized by 0.015 mm, had been cooled and inserted. The various hoop strain measurements are shown in Fig. 5(a). The best estimate of the three principal stresses (Fig. 5(b)) were obtained from a Bayesian best

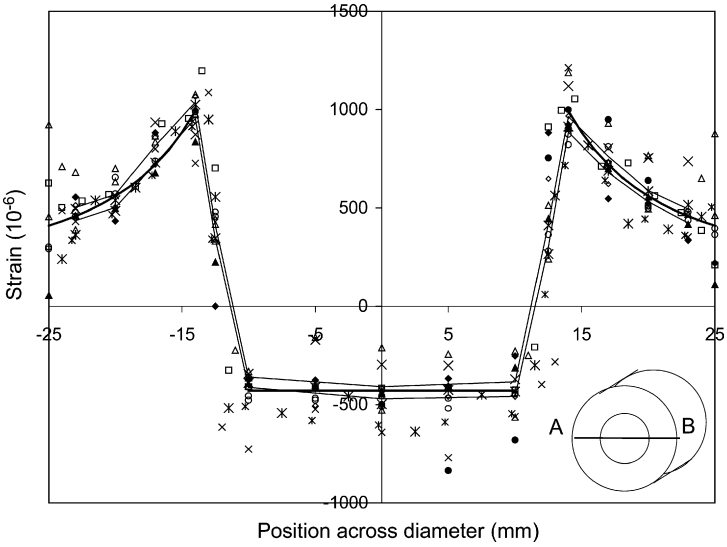

(a)

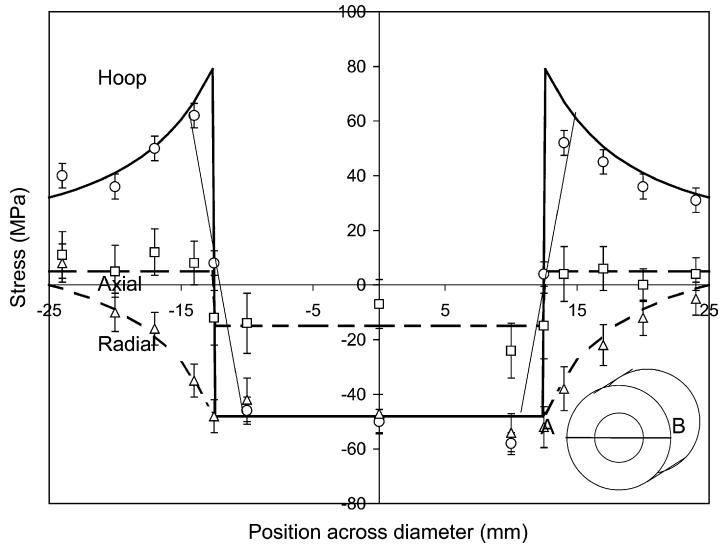

(b)

Fig. 5. (a) The measurements (points) of the hoop strain component, obtained at 18 facilities world-wide on two identical shrink fit Al plug samples, across a mid-plane diameter (A–B in inset). The bold line shows the averaged strain variation, and the other lines the uncertainties of ± one standard deviation, about $\pm 75 \times 10^{-6}$ from the mean. Note how surface effects lead to larger errors at the edges of the ring. (b) The best estimate of the three principal stresses (points) obtained from the measured principal strains, compared with results of an analytical calculation (bold line) assuming an interference between ring and plug of 21.5 μm. The sloping lines at the interface represent smoothing of the calculated stress variation by the instrumental gauge volume [39].

fit to all the data. The overall standard error of the results was 75×10^{-6} in strain and 7 MPa in stress, giving confidence that repeatable data can be obtained [39].

6. Example applications

The measurement of strain by neutron diffraction has contributed to increasing our understanding of a very wide range of problems. The examples described below exemplify the unique capabilities of the method and illustrate how it can provide insights ranging from the activation of basic slip mechanisms at the atomic scale, to stresses in full-scale engineering components.

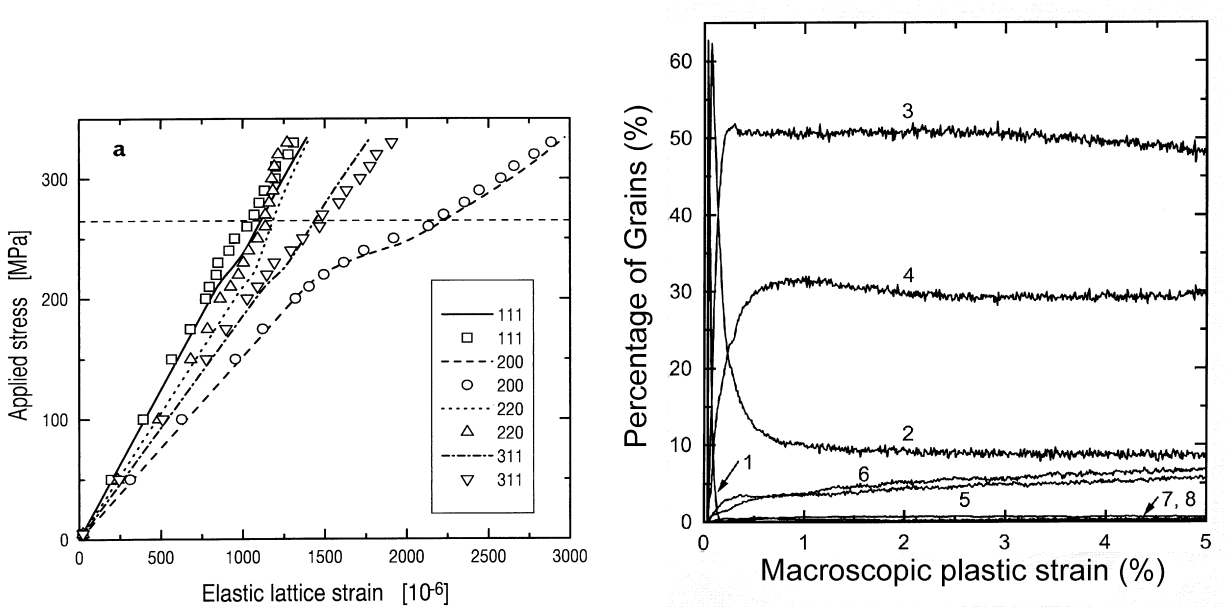

(a) (b)

Fig. 6. (a) A comparison between the lattice strains predicted under tensile loading for certain *hkl* planes in stainless steel as predicted by a self-consistent prediction (lines) compared with direct measurements by neutron diffraction (data points). The horizontal dashed line at ∼265 MPa represents the 0.2% proof macroscopic yield stress [54,55]. (b) The percentage of grains having different numbers of active slip systems shown, as a result of macroscopic uniaxial plastic strain for a typical fcc material [51].

6.1. Elucidating basic slip mechanisms

The basic slip mechanisms for cubic materials operating in a single crystal have been known for many years. The interaction/competition between them within neighbouring grains in a polycrystal due to mutual constraint during plastic deformation is a very important issue in deformed metals affecting texture (preferred orientation) [40,41], hardening in the stress-strain curve, recrystallisation [42] and ultimately failure. To explain how different grains interact, a number of modelling strategies have been developed. The early models of Taylor and Sachs [43,44] are plastic analogues of the Voigt and Reuss models for elastic behaviour, and serve as bounds for the real behaviour of a polycrystal. More recently elasto-plastic self-consistent (EPSC) modelling schemes have considered the constraint of an effective average medium on individual grains [30,45]. At some computational cost, finite element (FE) modelling enables one to consider the effect on each grain, or sub-volume of a grain, of its specific neighbours [42,46,47], as well as to model the development of internal strains [48,49]. Because neutron diffraction can provide information about the development of the *hkl* specific intergranular strains, it has become a major tool in the development of such models [30,50–53]. In Fig. 6(a) the *hkl* specific lattice strains generated during tensile deformation for stainless steel are well predicted using an EPSC model [54,55], from which the number of slip systems active in each grain as a function of strain can be inferred (Fig. 6(b)).

The situation is not so well advanced for other crystal systems. For hexagonal crystal structures the number of available slip systems is much reduced. This increases the propensity for intergranular stress and the occurrence of plastic deformation by twinning. The extent of twinning varies greatly from material to material according to the stacking fault energy. Neutron diffraction is providing much useful information, enabling modellers to identify the energies of the various slip and twinning mechanisms for Zr [56], Hf [57], Ti [58], Mg [59,60] and Be [61]. A good example of this is provided by the data collected for in-plane tension of Mg shown in Fig. 7.

6.2. Transformations in smart materials

Newnham states [62]: "*One of the qualities that distinguishes living systems from inanimate matter is the ability to adapt to changes in the environment. Smart materials have the ability to perform both sensing and actuating functions*

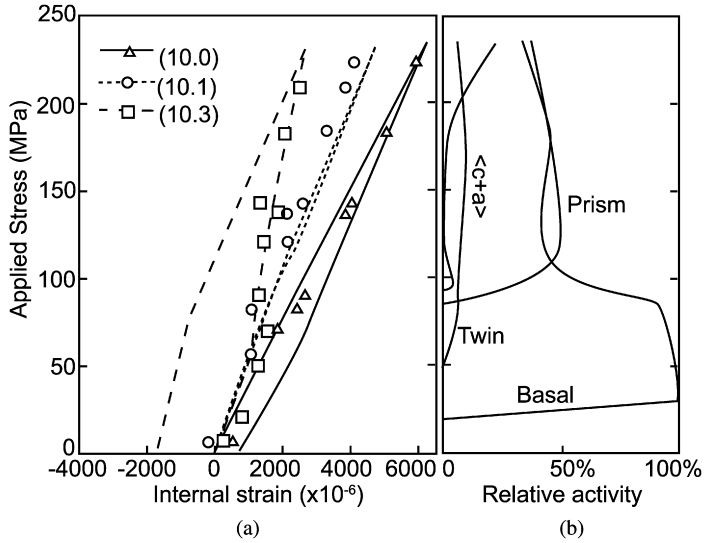

Fig. 7. (a) Lattice strain development for three (*hkl*) planes families oriented with their plane normals parallel to the applied stress axis for in-plane tension of Mg. Symbols denote strain measurements while the lines correspond to simulations; (b) predicted relative activity of the various slip and twinning mechanisms [59].

and are, therefore, capable of imitating this rudimentary aspect of life." Many 'smart' materials rely on solid state transformations that occur displacively. These transformations are characterised by a rapid distortion of the crystal lattice from one structure to another, thereby generating a misfit between the transformed and untransformed regions which may give rise to residual stresses [63] as well as a sudden macroscopic shape change.

A very wide range of structural transformations have been studied by neutron diffraction, especially using the tof method for the reasons discussed above. In many cases these have benefited from the fact that it is relatively straightforward to install rigs to activate the structural transformation via electric [64] or magnetic field [65], applied load [66,67], pressure [68,69] or temperature [70] in situ. Indeed stroboscopic methods have been developed to counter the rather slow (>1 s) data acquisition rates traditionally associated with neutron diffraction to study ferroelectric transitions under changing electric fields at the millisecond timescale [64].

Diffraction can provide phase fractions, variant selection and internal stresses non-destructively as a function of the environment. Furthermore, these parameters can be correlated against external parameters such as the macroscopic actuation of a ferroelectric component. A good example of the information that can be obtained is provided by a study of the stress-induced martensitic transformation and variant change in Fe-30.5 at % Pd [70]. This alloy demonstrates very little thermal hysteresis in that the temperatures at which martensite starts to form during cooling, and the reverse transformation finishes during heating are 16 and 17 °C, respectively. Fig. 8 shows the variation with applied stress of the integrated intensities of the $(200)_a$, $(311)_a$ and $(220)_a$ austenite reflections parallel to the loading direction, and the corresponding martensite reflections as a function of applied load. For each reflection set, the reduction in austenite reflection intensity is accompanied by an approximately equal increase in martensite reflection intensity. At a given applied stress, the fractional reduction in intensity of the austenite reflections increases in the order $(220)_a$ to $(311)_a$ to $(200)_a$. This indicates that the tensile stress induces transformation most readily in grains oriented such that a ⟨100⟩ direction lies parallel to the tensile axis. Transformation is less favoured as the angle between ⟨100⟩ and the tensile axis increases. Since the formation of a martensite plate causes greatest elongation along a ⟨100⟩ direction, the potential energy is most greatly reduced by plate formation in a 100-type grain.

6.3. Interphase stresses in composite materials

The presence of residual, or internal, stresses must be taken into account when considering the mechanical properties of almost any system that is mechanically inhomogeneous. This is especially true of composite materials. For the majority of composites, the second phase is added with a view to bringing to the composite attributes not present in the matrix alone, for example, stiffness, strength, low thermal expansivity, etc. The degree of success to which this is

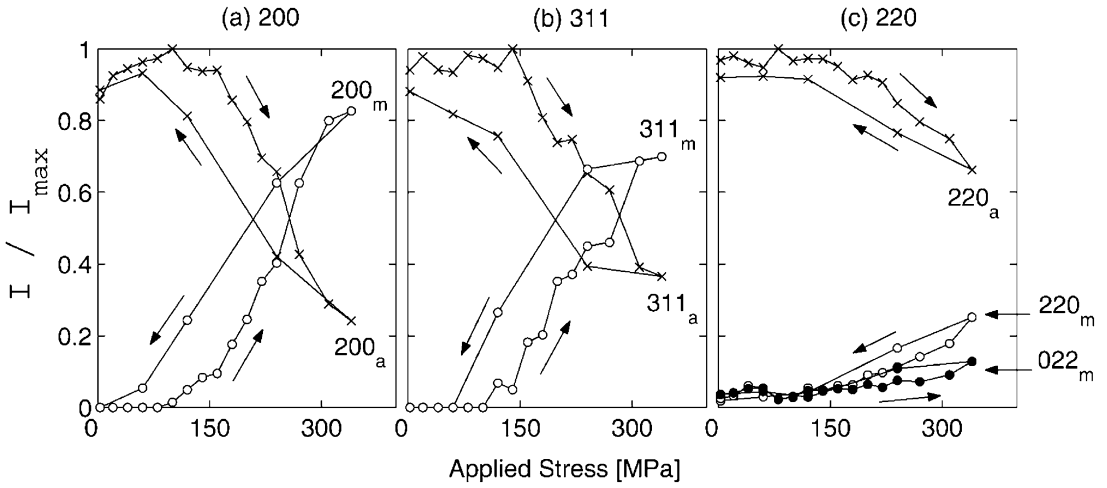

Fig. 8. Variation of integrated peak intensities for *hkl* planes oriented normal to the applied stress during stress-induced transformation at 24 °C. Crosses—austenite reflections; circles—martensite reflections with same Miller indices, as labelled for each plot. Intensities are scaled by the fourth power of the d-spacing, and normalised with respect to the maximum intensity of the appropriate austenite reflection. Arrows indicate the loading and unloading curves [70].

achieved is, at least partly, dependent on the generation of internal stresses between the phases. If the behaviour of a composite is to be optimised for a particular application, it is therefore important to be able to monitor the levels of internal stress and thus to learn how to tailor them to advantage.

The average stress in each phase of a composite can have many of the characteristics of a long range stress field, while being a microscale effect. To illustrate this type of residual stress, consider the cooling of a matrix (phase 1) containing a single inclusion of another phase (phase 2). Except in the unlikely event that the two phases had the same coefficients of thermal expansion, this would create a type II stress. The stress field from a single inclusion is essentially insignificant at a distance beyond a few particle diameters. However, if the matrix contains many inclusions of phase 2 then the stress would self-equilibrate over volumes larger than some characteristic size, V_o, sufficiently large that it contained phase volume fractions corresponding to those found in the composite overall (f_1 and f_2):

$$f_1\langle\sigma_1\rangle + f_2\langle\sigma_2\rangle = 0 \tag{6}$$

where $\langle\sigma_1\rangle$ and $\langle\sigma_2\rangle$ are termed mean phase microstresses by the present author [9,71]. Since the total stress averages to zero over macroscopic length scales, the stress is correctly classified as a type II stress field and would be invisible to destructive stress measurement techniques. Diffraction on the other hand would measure a tensile or compressive stress depending on the phase. A good example of this effect is provided by the thermal stresses that arise as an SiC whisker containing Al matrix is heated/cooled (see Fig. 9).

In practice there are a host of ways in which stresses can be introduced into composite materials. Most commonly, one must consider:

- Elastic mismatch stresses [72];
- Thermal misfits metal matrix–ceramic particle [73–75], ceramic matrix [76]; hard metal (cermet) [77] and metal–metal [78] composite systems;
- Plastic misfits of the matrix [71,79] or matrix and fibres for co-deforming systems [80,81];
- Reinforcement failure or debonding [82];
- Transformations [83,84].

A stroboscopic method has been developed for studying how stresses regenerate under thermal cycling [85].

6.4. From test samples to full-scale trials

Neutron diffraction allows one to study real components under realistic conditions of temperature, load or environment. This is very important to the engineer because it is not always possible to reduce an engineering problem

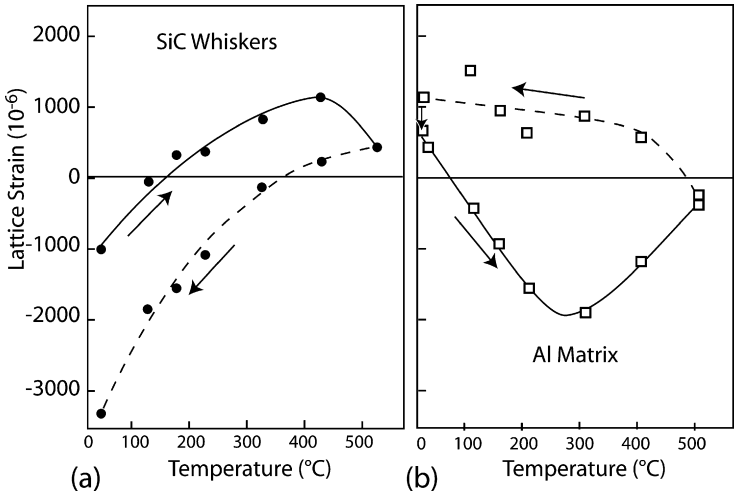

Fig. 9. Neutron strain measurements of the mean Al and SiC 111 lattice strain components parallel to the whisker alignment direction in (a) the whiskers, and (b) the matrix, for an Al/5%SiC_W, composite made over a thermal cycle. The arrows show the heating (solid) and cooling (dashed) curves [73].

down to simple test-pieces. Sometimes, after extensive trials on sub-scale systems the structural integrity issue must be transferred to the full-scale system before implementing new industrial processes. A good example of this is the introduction of inertia welding into aeroengine production [86].

Inertia friction welding (IFW) is a solid state welding method suitable for joining axi-symmetric components such as discs. In IFW, one of the work-pieces is connected to a flywheel and the other is held stationary. The flywheel is accelerated to a predetermined rotational speed, then disengaged and the work-pieces are forced together under pressure. The kinetic energy stored in the rotating flywheel is dissipated as heat through friction/shearing at the weld interface. When the flywheel rotation stops, the axial force (pressure) between the components is maintained, and a solid state bond is formed at the softened interface. As a solid state process, inertia welding avoids the problems usually associated with melting and re-solidification and allows for the formation of a narrow heat affected zone. Udimet 720Li is one of the latest generation of high performance nickel-base superalloys having a significantly higher volume fraction of γ' phase than conventional superalloys. It is very difficult to weld and prone to micro-cracking upon solidification during conventional fusion welding. Friction welding however is proving to be a very efficient technique.

A series of sub-scale 143 mm diameter rings (8 mm wall thickness at weld) were inertia friction welded (Fig. 10(a)). One was studied in the as-welded condition and the others were post-weld heat treated by ramp heating/cooling and exposed at 760 °C for various dwell times. Neutron diffraction measurements were conducted to quantify residual stress levels. Based on the results obtained for these small scale specimens, a full scale high pressure aeroengine compressor drum-drive cone assembly (∼500 mm diameter and 8 mm wall thickness) was inertia friction welded under similar conditions and post-weld heat treated (760 °C/8 h). A photograph of the drum-drive cone assembly during measurement at the ENGIN-X facility is shown in Fig. 10(e).

Notably; the hoop stresses in the sub-scale sample after welding are significantly tensile (Fig. 10(b)) gradually falling away with distance (z) from the weld-line. A decrease in the hoop stress occurs immediately upon heating to 760 °C (Fig. 10(c)); prolonged exposure brings about a reduction to approximately 55% of the as-welded state towards both inner and outer walls (Fig. 10(d)). The stresses in the full-scale assembly after 8 hours are very similar, if not a little lower, than those in the corresponding sub-scale test-piece (Fig. 10(f)).

7. Conclusions

Since the first dedicated instrument in the mid 1990s [87] residual stress measurement by neutron diffraction has become a mature discipline with recognised standards for repeatable measurement [31]. Taken together with the complementary synchrotron method it can provide non-destructive evaluation for the introduction of new process

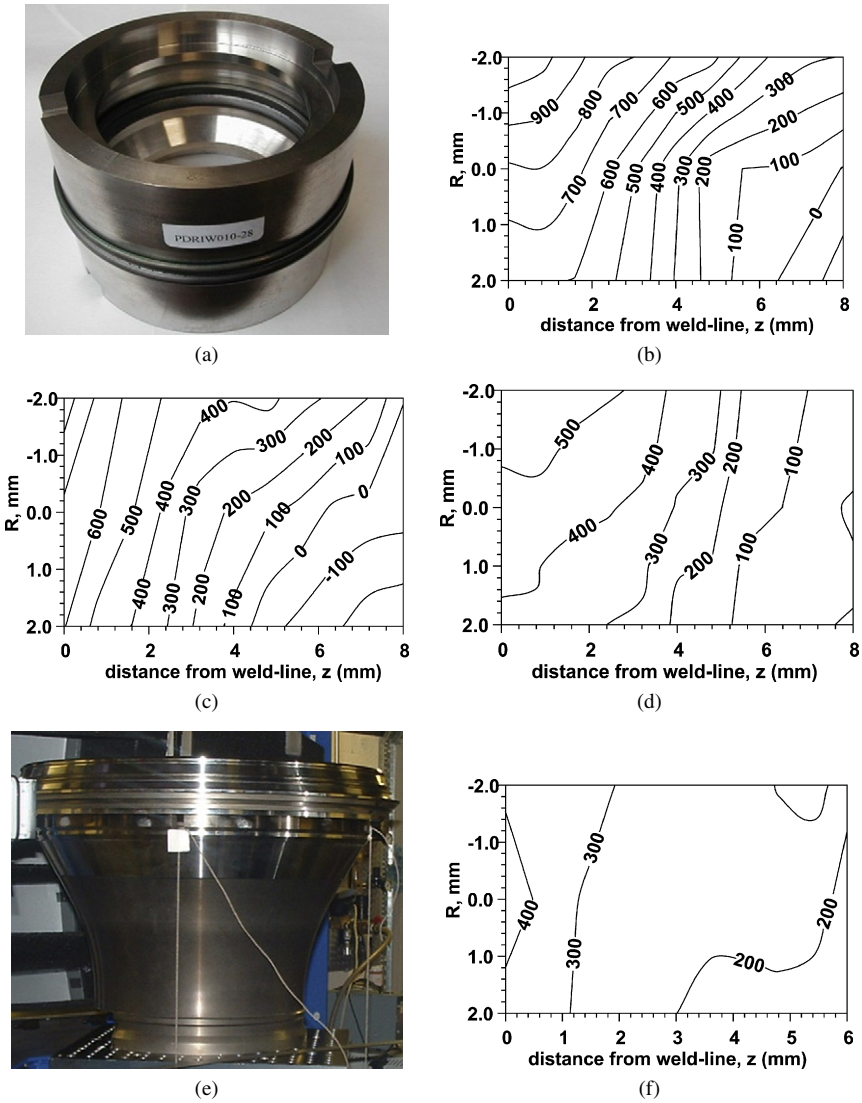

Fig. 10. (a) Sub-scale (143 mm diameter) inertia welded prototype. Sub-scale hoop stresses measured on SALSA at the ILL (inner wall at $R = -4$, outer wall at $R = 4$ mm) for (b) as-welded, (c) 0 h, 760 °C, (d) 8 h, 760 °C for the sub-scale, (e) full-scale (500 mm diameter) high pressure aeroengine compressor drum - drive cone assembly and (f) 8 h, 760 °C for the full-scale weld [86].

technologies, or for structural integrity assessment at the component or plant scale. Recently, neutrons have even been used to study welding process induced stresses in situ [88]. At the device level, neutron diffraction can provide information into the activation of smart transformations, while at the material level it delivers phase or grain family information for optimising the performance of alloys and composites. With the increasing number and performance of dedicated neutron strain measurement instruments around the world there is no doubt that neutron diffraction will continue to make a significant contribution to basic science and applied engineering over the coming years.

Acknowledgements

I am grateful for the help of M. Karadge, M. Preuss, A. Steuwer, the FaME38 team and all the instrument scientists who make engineering and materials science measurements possible at neutron facilities across the world. I am also grateful for the support of a Royal Society-Wolfson Merit Award.

References

[1] W.H. Bragg, Proc. Roy. Soc. 89A (1913) 246–248, 8–77.
[2] H.H. Lester, R.H. Aborn, Army Ordnance 6 (1925) 120–127, 200–207, 83–87, 364–369.
[3] A.E. van Arkel, Physica B 5 (1925) 208–212.
[4] A.F. Joffe, M.V. Kirpitcheva, Phil. Mag. 43 (1922) 204–206.
[5] V. Hauk, Structural and Residual Stress Analysis by Non-Destructive Methods, Elsevier Science B.V., Oxford, 1997.
[6] A.J. Allen, C. Andreani, M.T. Hutchings, C.G. Windsor, NDT International 15 (1981) 249–254.
[7] L. Pintschovius, V. Jung, E. Macherauch, R. Schäfer, O. Vöhringer, In: E. Kula, V. Weiss (Eds.), Residual Stress and Stress Relaxation, Proceedings of the 28th Army Materials Research Conference, 1981 July, Lake Placid, Plenum, New York, pp. 467–482.
[8] A.D. Krawitz, J.E. Brune, M.J. Schmank, In: E. Kula, V. Weiss (Eds.), Residual Stress and Stress Relaxation, Proceedings of the 28th Army Materials Research Conference, 1981 July, Lake Placid, Plenum, New York, pp. 139–155.
[9] M.T. Hutchings, P.J. Withers, T.M. Holden, T. Lorentzen, Introduction to the Characterisation of Residual Stresses by Neutron Diffraction, CRC Press, Taylor & Francis, London, 2005.
[10] M.T. Hutchings, A.D. Krawitz (Eds.), Measurement of Residual and Applied Stress Using Neutron Diffraction, NATO ASI Series E Applied Science, vol. 216, Kluwer Academic Publishers, Dordrecht, 1992.
[11] A.D. Krawitz, T.M. Holden, MRS Bull. XV (1990) 57–64.
[12] J.L. Lebrun, P. Gergaud, V. Ji, M. Belassel, J. de Physique IV (1995) 265–268.
[13] P.J. Withers, M. Preuss, P.J. Webster, D.J. Hughes, A.M. Korsunsky, Materials Sci. Forum (ECRSV) 404–407 (2002) 1–10.
[14] P.J. Withers, in: K.H.J. Buschow, R.W. Cahn, M.C. Flemings, B. Ilschner, E.J. Kramer, S. Mahajan (Eds.), Encyclopedia of Materials: Science & Technology, Elsevier, Oxford, 2001, pp. 8158–8170.
[15] T. Pirling, G. Bruno, P.J. Withers, Mat. Sci. Eng. 437A (2006) 139–144.
[16] R.P. Schneider, T. Poeste, H. Freydank, M. Hofmann, in: Measurement of Residual Stress in Materials Using Neutrons, 2005, Vienna, Int. Atomic Energy Agency; IAEA-TECDOC-1457, pp. 61–70.
[17] P. Mikula, M. Vrána, P. Lukáš, in: Measurement of Residual Stress in Materials Using Neutrons, 2005, Vienna, Int. Atomic Energy Agency; IAEA-TECDOC-1457, pp. 19–27.
[18] T. Holden, A.D. Krawitz, I. Anderson, Journal of Metals 58 (2006) 64–67.
[19] A.G. Youtsos, in: Measurement of Residual Stress in Materials Using Neutrons, 2005, Vienna, Int. Atomic Energy Agency; IAEA-TECDOC-1457, pp. 33–50.
[20] M. Ceretti, R. Coppola, A. Lodini, M. Perrin, F. Rustichelli, Physica B 213 (1995) 803–805.
[21] T. Gyula, in: Measurement of Residual Stress in Materials Using Neutrons, 2005, Vienna, Int. Atomic Energy Agency; IAEA-TECDOC-1457, pp. 71–79.
[22] T. Gnäupel-Herold, in: Measurement of Residual Stress in Materials Using Neutrons, 2005, Vienna, Int. Atomic Energy Agency; IAEA-TECDOC-1457, pp. 81–90.
[23] P.J. Withers, M.W. Johnson, J.S. Wright, Physica B 292 (2000) 273–285.
[24] M.R. Daymond, M.A.M. Bourke, R.B. Von Dreele, B. Clausen, T. Lorentzen, J. Appl. Phys. 82 (4) (1997) 1554–1556.
[25] L.E. Edwards, P.J. Withers, M.R. Daymond, in: G.A. Webster (Ed.), 6th International Conference on Residual Stress, ISBN 1-86125-123-8, Institute of Materials, Oxford, 2000, pp. 1116–1123.
[26] U. Stuhr, H. Spitzer, J. Egger, A. Hofer, P. Rasmussen, D. Graf, A. Bollhalder, M. Schild, G. Bauer, W. Wagner, Nuclear Instrum. Methods Phys. Res. A 545 (2005) 330–338.
[27] M.A.M. Bourke, D.C. Dunand, E. Ustundag, Appl. Phys. A—Mater. Sci. Process. 74 (2002) S1707–S1709.
[28] X.L. Wang, Journal of Metals 58 (2006) 52–57.
[29] J.F. Nye, Physical Properties of Crystals—Their Representation by Tensors and Matrices, Clarendon, Oxford, 1985.
[30] A. Baczmanski, K. Wierzbanowski, J. Tarasiuk, M. Ceretti, A. Lodini, Revue de Metallurgie—Cahiers d'informations techniques 94 (1997) 1467–1474.
[31] G.A. Webster (Ed.), ISO/TTA3 Technology Trends Assessment, Geneva 20, Switzerland, 2001.
[32] P.J. Withers, J. Appl. Cryst. 37 (2004) 596–606.
[33] W. Reimers, M. Broda, B. Brusch, D. Dantz, K.-D. Liss, A. Pyzalla, T. Schmackers, T. Tschentscher, J. Nondest. Eval. 17 (1998) 129–140.
[34] P.J. Withers, in: M.E. Fitzpatrick, A. Lodini (Eds.), Analysis of Residual Stress by Diffraction using Neutron and Synchrotron Radiation, Taylor & Francis, London, 2003, pp. 170–189.
[35] H.J. Stone, H.K.D.H. Bhadeshia, P.J. Withers, Mat. Sci. Forum (2008), in press. Paper was presented at 4th Meca SENS in Vienna.
[36] A. Steuwer, J.R. Santisteban, M. Turski, P.J. Withers, T. Buslaps, J. Appl. Cryst. 37 (2005) 883–889.
[37] A. Steuwer, M. Rahman, M.E. Fitzpatrick, L. Edwards, P.J. Withers, The evolution of residual and crack-tip stresses during a fatigue overload, Acta. Mater. (2007), in preparation.
[38] S. Ganguly, M.E. Fitzpatrick, L. Edwards, Met. Mat. Trans. A 37 (2006) 411–420.
[39] M.R. Daymond, M.W. Johnson, D.S. Sivia, J. Strain Anal. Engrg. Design 37 (2002) 73–85.
[40] G.B. Sarma, P.R. Dawson, Internat. J. Plasticity 12 (1996) 1023–1054.
[41] P. Van Houtte, A.K. Kanjarla, A. Van Bael, M. Seefeldt, L. Delannay, Europ. J. Mech. A—Solids 25 (2006) 634–648.
[42] P. Bate, Phil. Trans. Royal Soc. London Ser. A—Math. Phys. Engrg. Sci. 357 (1999) 1589–1601.
[43] G.I. Taylor, J. Inst. Met. 62 (1938) 307–324.
[44] G. Sachs, Z. VDI 72 (1928) 734–736.
[45] R.A. Lebensohn, C.N. Tomé, Acta Metall. Mater. 41 (1993) 2611–2624.

[46] A.J. Beaudoin, K.K. Mathur, P.R. Dawson, G.C. Johnson, Int. J. Plasticity 9 (1993) 833.
[47] R. Becker, Acta Metall. Mater. 39 (1991) 1211–1230.
[48] N. Barton, P. Dawson, M. Miller, J. Eng. Mat. Tech.—Trans. ASME 121 (1999) 230–239.
[49] P. Dawson, D. Boyce, S. MacEwen, R. Rogge, Mat. Sci. Eng. A 313 (2001) 123–144.
[50] L. Delannay, R.E. Loge, Y. Chastel, P.V. Houte, Acta Mater. 50 (2002) 5127–5138.
[51] B. Clausen, T. Lorentzen, T. Leffers, Acta Mater. 46 (1998) 3087–3098.
[52] P.A. Turner, C.N. Tome, Acta Metall. 42 (1994) 4143–4153.
[53] P. Dawson, D. Boyce, S. MacEwen, R. Rogge, Met. Mat. Trans. A 31 (2000) 1543–1555.
[54] B. Clausen, in: Risø National Laboratory, Risø-R-985(EN), Roskilde, Denmark, 1997.
[55] B. Clausen, T. Lorentzen, M.A.M. Bourke, M.R. Daymond, Mat. Sci. & Eng. A 259 (1999) 17–24.
[56] G.C. Kaschner, C.N. Tome, I.J. Beyerlein, S.C. Vogel, D.W. Brown, R.J. McCabe, Acta Mater. 54 (2006) 2887–2896.
[57] C.A. Yablinsky, E.K. Cerreta, G.T. Gray, D.W. Brown, S.C. Vogel, Met. Mat. Trans. A 37 (2006) 1907–1915.
[58] E.C. Oliver, M.R. Daymond, J. Quinta da Fonseca, P.J. Withers, J. Neutron Res. 12 (2004) 33–37.
[59] S.R. Agnew, C.N. Tome, D.W. Brown, T.M. Holden, S.C. Vogel, Scripta Mater. 48 (2003) 1003–1008.
[60] E.C. Oliver, M.R. Daymond, P.J. Withers, in: Materials Science Forum (ICOTOM 14), vol. 490–491, 2005, pp. 257–262.
[61] D.W. Brown, S.R. Agnew, S.P. Abeln, W.R. Blumenthal, M.A.M. Bourke, M.C. Mataya, C.N. Tome, S.C. Vogel, in: ICOTOM 14: Textures of Materials, Pts 1 and 2, 2005, pp. 1037–1042.
[62] R.E. Newnham, Acta Crystallogr. Sect. A 54 (1998) 729–737.
[63] T. Mori, P.J. Withers, in: K.H.J. Buschow, R.W. Cahn, M.C. Flemings, B. Ilschner, E.J. Kramer, S. Mahajan (Eds.), Encyclopedia of Materials: Science & Technology, Elsevier, Oxford, 2001, pp. 8113–8121.
[64] U. Steigenberger, G. Eckold, M. Hagen, Physica B—Condens. Matter 213 (1995) 1012–1016.
[65] N. Glavatska, G. Mogylnyy, S. Danilkin, D. Hohlwein, in: European Powder Diffraction EPDiC 8, 2004, pp. 397–400.
[66] P. Sittner, P. Lukas, D. Neov, M.R. Daymond, V. Novak, G.M. Swallowe, Mater. Sci. Eng. A 324 (2002) 225–234.
[67] E.H. Kisi, S.J. Kennedy, C.J. Howard, J. Amer. Ceram. Soc. 80 (1997) 621–628.
[68] E.H. Kisi, J. Amer. Ceram. Soc. 81 (1998) 741–745.
[69] H.G. Smith, R. Berliner, J.D. Jorgensen, J. Trivisonno, Phys. Rev. B 43 (1991) 4524–4526.
[70] E.C. Oliver, T. Mori, M.R. Daymond, P.J. Withers, Acta Mater. 51 (2003) 6453–6464.
[71] P.J. Withers, W.M. Stobbs, O.B. Pedersen, Acta Metall. 37 (1989) 3061–3084.
[72] A.J. Allen, M. Bourke, S. Dawes, M.T. Hutchings, P.J. Withers, Acta Metall. 40 (1992) 2361–2373.
[73] P.J. Withers, D.J. Jensen, H. Lilholt, W.M. Stobbs, in: F.L. Matthews, N.C.R. Buskell, J.M. Hodgkinson, J. Morton (Eds.), Proc. ICCM VI/ECCM2, Elsevier, London, 1987, pp. 255–264.
[74] M. Ceretti, C. Braham, J.L. Lebrun, J.P. Bonnafe, M. Perrin, A. Lodini, Experimental Techniques 20 (1996) 14–18.
[75] R. Levy-Tubiana, A. Baczmanski, A. Lodini, Mater. Sci. Eng. A 341 (2003) 74–86.
[76] S. Majumdar, D.S. Kupperman, J.P. Singh, J. Am. Cer. Soc. 71 (1988) 858–863.
[77] C.M. Weisbrook, A.D. Krawitz, Mat. Sci. Eng. A 209 (1996) 318–328.
[78] R.J. Klassen, K.T. Conlon, J.T. Wood, Scripta Mater. 48 (2003) 385–389.
[79] N. Shi, R.J. Arsenault, A.D. Krawitz, L.F. Smith, Met. Trans. Ser. A 24 (1993) 187–196.
[80] K.L. Lee, A.F. Whitehouse, P.J. Withers, M.R. Daymond, Mat. Sci. Eng. A 348 (2003) 208–216.
[81] C.W. Sinclair, G. Saada, J.D. Embury, Philos. Magazine 86 (2006) 4081–4098.
[82] C.A. Lewis, P.J. Withers, Acta Metall. Mater. 43 (1995) 3685–3699.
[83] W.D. Armstrong, T. Lorentzen, P. Brøndsted, P.H. Larsen, Acta. Mater. 46 (1998) 3455–3466.
[84] D.C. Dunand, D. Mari, M.A.M. Bourke, J.A. Roberts, Met. & Mat. Trans. A 27 (1996) 2820–2836.
[85] M.R. Daymond, P.J. Withers, Scripta Metall. Mater. 35 (1996) 717–720.
[86] M. Karadge, G.M. Regino, B. Grant, A. Hoerling, P.J. Withers, M. Preuss, A.M. Korsunsky, G. Baxter, Mater. Metal. Trans. (2007), submitted for publication.
[87] M.W. Johnson, L. Edwards, P.J. Withers, Physica B 234 (1997) 1141–1143.
[88] W. Woo, Z. Feng, X.-L. Wang, K. An, W.B. Bailey, S.A. David, C.R. Hubbard, H. Choo, Mat. Sci. Forum 524–525 (2006) 387–392.